

## Modeling Active Contraction and Relaxation of Left Ventricle Using Different Zero-load Diastole and Systole Geometries for Better Material Parameter Estimation and Stress/Strain Calculations

Longling Fan<sup>1§</sup>, Jing Yao<sup>2§</sup>, Chun Yang<sup>3</sup>, Di Xu<sup>2</sup>, Dalin Tang<sup>1,4\*</sup>

**Abstract:** Modeling ventricle active contraction based on in vivo data is extremely challenging because of complex ventricle geometry, dynamic heart motion and active contraction where the reference geometry (zero-stress geometry) changes constantly. A new modeling approach using different diastole and systole zero-load geometries was introduced to handle the changing zero-load geometries for more accurate stress/strain calculations. Echo image data were acquired from 5 patients with infarction (Infarct Group) and 10 without (Non-Infarcted Group). Echo-based computational two-layer left ventricle models using one zero-load geometry (1G) and two zero-load geometries (2G) were constructed. Material parameter values in Mooney-Rivlin models were adjusted to match echo volume data. Effective Young's moduli (YM) were calculated for easy comparison. For diastole phase, begin-filling (BF) mean YM value in the fiber direction ( $YM_f$ ) was 738% higher than its end-diastole (ED) value (645.39 kPa vs. 76.97 kPa,  $p=3.38E-06$ ). For systole phase, end-systole (ES)  $YM_f$  was 903% higher than its begin-ejection (BE) value (1025.10 kPa vs. 102.11 kPa,  $p=6.10E-05$ ). Comparing systolic and diastolic material properties, ES  $YM_f$  was 59% higher than its BF value (1025.10 kPa vs. 645.39 kPa,  $p=0.0002$ ). BE mean stress value was 514% higher than its ED value (299.69 kPa vs. 48.81 kPa,  $p=3.39E-06$ ), while BE mean strain value was 31.5% higher than its ED value (0.9417 vs. 0.7162,  $p=0.004$ ). Similarly, ES mean stress value was 562% higher than its BF value (19.74 kPa vs. 2.98 kPa,  $p=6.22E-05$ ), and ES mean strain value was 264% higher than its BF value (0.1985 vs. 0.0546,  $p=3.42E-06$ ). 2G models improved over 1G model limitations and may provide better material parameter estimation and stress/strain calculations.

---

<sup>1</sup> Department of Mathematics, Southeast University, Nanjing, 210096, China.

<sup>2</sup> Department of Cardiology, First Affiliated Hospital of Nanjing Medical University, Nanjing 210029, China.

<sup>3</sup> Network Technology Research Institute, China United Network Communications Co., Ltd., Beijing, 100048, China.

<sup>4</sup> Mathematical Sciences Department, Worcester Polytechnic Institute, MA 01609 USA.

These authors contributed equally to this work

\*Corresponding author: Dalin Tang, e-mail: dtang@wpi.edu.

**Keywords:** Active contraction, ventricle model, ventricle material properties, ventricle stress, ventricle strain, ventricle material parameter.

## 1 Introduction

Obtaining myocardium material properties in vivo is of fundamental importance for ventricle modeling, mechanical analysis and accurate stress/strain calculations for correct understanding of cardiac functions [Holmes and Costa(2006), Fomovsky, Macadangdang, Ailawadi, and Holmes(2011)]. By using in vivo ventricle volume and pressure conditions, it is possible to determine myocardium material properties with some inverse method or iterative method [Fan, Yao, Yang, et al. (2015)]. However, it is well known that ventricle function involves active contraction and relaxation, which lead to different zero-stress ventricle geometries for diastole and systole phases. Due to ventricle active contraction, its zero-stress systole geometry is smaller than its zero-stress diastole geometry, even though those zero-stress geometries are not observable under in vivo conditions. To properly model ventricle active contraction and relaxation and obtain correct material properties and stress/strain calculations, different zero-stress geometries should be used for systole and diastole phases, respectively. From mechanical point of view, zero-stress ventricle geometry information is required for its stress/strain calculations. An approach using two zero-load geometries (2G) is proposed to model ventricle cardiac motion: one zero-load ventricle geometry is used to model the diastole phase, another zero-load ventricle geometry is used to model the systole phase. Zero-load geometry is the ventricle geometry when its internal pressure is zero. It should be noted that “zero-stress” and “zero-load” are two different concepts. Zero-load geometries are used as an approximation since zero-stress state is really hard to get. Zero-load geometries are what we need for model construction purposes.

Active contraction is caused by sarcomere shortening which leads to increased strain and stress (called active strain and stress) when ventricle transitions from end-filling to begin-ejection with its volume unchanged. Peskin pioneered active heart modeling effort and simulated blood flow in a pumping heart with his immersed boundary method [Peskin (1997)]. McCulloch, Hunter, Kerckhoffs and many other authors have made great contributions to passive and active ventricle modeling, such as the Physiome Project and the Continuity package [McCulloch, Waldman, Rogers, et al. (1992); McCulloch(2007), Hunter, Pullan, and Smail (2003); Kerckhoffs, Healy, Usyk, et al. (2006), Pfeiffer, Tangney, Omens JH, et al. (2014)]. Guccione et al. proposed the constitutive relations for active stress in cardiac muscle and developed three active tension models [Guccione and McCulloch(1993a), Guccione, Waldman, and McCulloch(1993b)]. Liu et al. developed a dynamic cardiac elastography framework to assess the anisotropic viscoelastic passive properties and active contractility of myocardial tissues [Liu, Wang, and Sun(2006)]. Wang et al. modeled the systolic mechanics and optimized the activation parameters by matching the pressure-volume relation established from the pressure record match echo-measureding [Wang, Lam, Ennis, et al. (2010)]. Rossi et al. deal with the establishment, implementation, and testing of an orthotropic model for cardiac contraction on the basis of an active strain decomposition [Rossi, Ruiz-Baier, Pavarino, et al. (2012)]. Pezzuto

and Ambrosi focus on the contraction of the left ventricle (LV) in a finite elasticity framework, adopting the “prolate ellipsoid” geometry and the invariants-based strain energy [Ambrosi and Pezzuto(2012)]dynamic model for the mechanical behaviour of LV [Moulton and Secomb(2013)].

Considerable effort has been devoted to quantifying heart tissue mechanical properties and fiber orientations mostly using animal models [Costa, Takayama, McCulloch, et al. 1999); Humphrey, Strumpf, and Yin(1999); Nash and Hunter(2000); Rogers and McCulloch(1994); Sacks and Chuong (1993); Takayama, Costa, and Covell(2002)]. Our group introduced patient-specific cardiac magnetic resonance (CMR)-based right ventricle/left ventricle models with fluid-structure interactions with various surgical design and potential applications [Tang, Yang, Geva, et al. (2008); Tang, Yang, Geva, et al. (2010); Tang, Yang, Geva, et al. (2011), Tang, del Nido, Yang, et al. (2016)].

In this paper, a new modeling approach using different systole and diastole zero-load geometries was introduced to properly model active contraction and relaxation and obtain ventricle diastole and systole material parameter values, stress and strain conditions. New models were constructed for 15 patients and results were compared with our previously published one-geometry models [Fan, Yao, Yang, et al. (2015)].

**2 Method**

**2.1 3D echo data acquisition**

Patients were recruited to participate in this study with written consent obtained at the First Affiliated Hospital of Nanjing Medical University, Nanjing, China from all participants (n=15, 11 males, mean age 58.9 years). Five patients had recent infarction (Infarct Group, IG) and ten patients did not have infarction (Non-Infarcted Group, NIG). Basic patient information is given in Table 1. Details of the data acquisition procedures were previously described [Fan, Yao, Yang, Tang, and Xu (2015)]. Figure 1 shows the echo images, diastole and systole zero-load geometries and re-constructed 3D pressurized geometries. In vivo LV pressure was recorded for modeling use (Fig. 2).

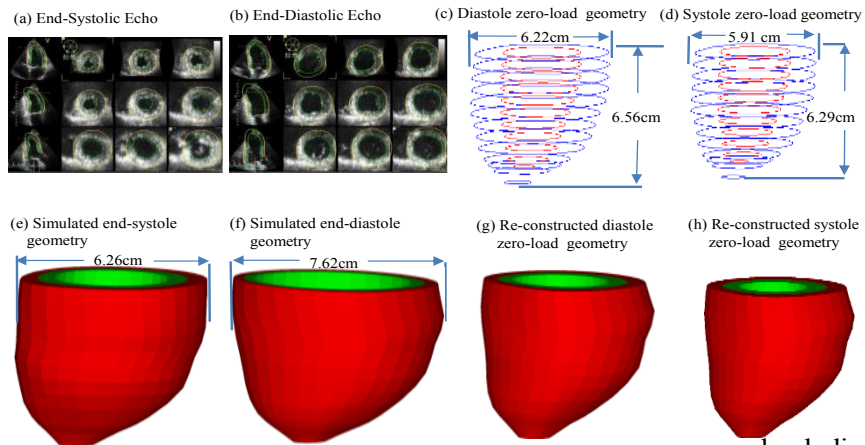
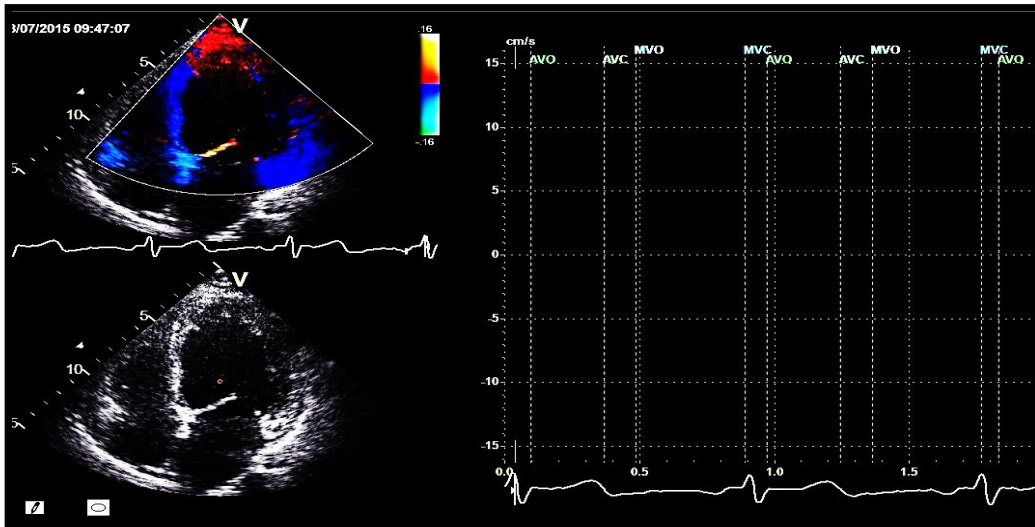


**Figure 1:** Echo image of a healthy volunteer (P1), contours, zero-load diastole and systole geometries and re-constructed pressurized geometries.

(a) Echo valve timing and Recorded electrocardiogram corresponding



(b) Recorded LV blood pressure profile



(c) LV pressure condition

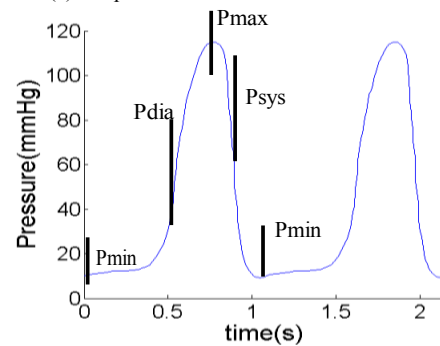


**Figure 2:** Recorded patient-specific electrocardiogram and pressure profiles, LV pressure condition used in the model with Pmin (Begin-Filling), Pdia (End-Filling), Pmax (Begin-Ejection), and Psys (End-Ejection) marked. AVO: Aortic valve open; AVC: Aortic valve close; MVO: Mitral valve open; MVC: Mitral valve close.

**Table 1:** Patient data and ventricle volume data. P1-P10 are people without infarction. P11-P15 are patients who had recent infarctions. F, Female; M, Male; EF, Ejection Fraction.

	Age	Sex	Pressure (mmHg)		Volume (ml)		EF (%)
			Min	Max	Min	Max	
P1	48	M	8	115	46	116	60
P2	43	F	10	130	46	120	61
P3	59	M	9	118	33	79	58
P4	43	M	8	115	51	120	58
P5	56	M	10	138	46	121	62
P6	49	F	10	130	25	72	65

P7	75	M	8	121	33	99	67
P8	55	F	9	121	43	94	54
P9	59	M	10	132	34	110	69
P10	62	M	9	128	41	99	59
Mean	54.9		9.1	124.8	39.8	103.0	61.3
$\pm$ SD	$\pm 9.75$		$\pm 0.88$	$\pm 7.87$	$\pm 8.15$	$\pm 17.5$	$\pm 4.57$
P11	60	M	10	121	103	176	42
P12	72	F	8	96	50	98	49
P13	73	M	9	105	115	193	40
P14	71	M	10	120	134	228	41
P15	58	M	9	110	70	147	53
Mean	66.8		9.2	110.4	94.4	168.4	45.0
$\pm$ SD	$\pm 7.19$		$\pm 0.84$	$\pm 10.5$	$\pm 34.0$	$\pm 49.1$	$\pm 5.70$

## 2.2 Modeling active contraction and expansion by using different zero-load diastole and systole geometries.

It is commonly accepted that a cardiac cycle may be divided into 4 phases, 2 in diastole (isovolumic relaxation followed by diastolic filling) and 2 in systole (isovolumic contraction followed by systolic ejection). A short description of the 4 phases is given below since this is the base for our 2-geometry models:

- *Phase 1.* Filling (diastole phase). This phase starts from begin-filling (BF) with minimum LV volume, pressure, stress and strain and ends at end-diastole (ED) with maximum LV volume. One zero-load geometry (diastole geometry) is used for this phase, corresponding to diastole zero-stress sarcomere length (SL). It should be noted that zero-stress status is a concept for stress/strain calculations. It is not observable in a living heart under in vivo conditions. At BF, mitral valve opens, LV volume increases; pressure increases; in vivo SL expands; strain and stress increases. Phase 1 ends when LV reaches its maximum volume under end-diastole pressure (denoted by  $P_{dia}$ ) which is lower than the maximum pressure condition. The zero-stress SL and zero-load LV geometry do not change in Phase 1.
- *Phase 2.* Isovolumic contraction: Both mitral (inlet) and aortic (outlet) valves are closed; LV volume has no change; zero-stress SL shortens (changing from diastole zero-stress length to systole zero-stress length, so no-load LV geometry changes from diastole no-load geometry to systole no-load geometry); however, this zero-stress sarcomere shortening is not physically observable since in vivo LV volume does not change in Phase 2. So, zero-stress SL shortening leads strain and stress increase (similar to the active tension in other models, but our model have both strain and stress increases); increased stress pushes pressure to maximum. This phase is short. This phase involves dynamic change of zero-stress sarcomere length equivalent to continuous change of zero-load LV geometry which is very difficult to implement. It was skipped in our model (which jumps from Phase 1 to Phase 3).
- *Phase 3.* Ejection (systole phase): This phase starts from begin-ejection (BE) with maximum volume, pressure, stress and strain and ends at end-systole (ES) with minimum

LV volume. The systole zero-load geometry is used for this phase, corresponding to systole zero-stress SL. At BE, aortic valve opens up and ejection starts; LV volume drops; in vivo SL shortens and strain decreases; pressure drops; stress drops. At end-systole, LV volume reaches its minimum, pressure drops to the end-systole pressure denoted as  $P_{sys}$ , which is greater than minimum pressure. Pressure will continue to drop in Phase 4 when systole zero-stress SL changes to diastole zero-stress SL.

- *Phase 4*. Isovolumic relaxation: Aortic valve closes (both valves closed); zero-stress SL relaxes from systole zero-stress length to diastole zero-stress length (reversing Phase 2); similar to the comments made in Phase 2, zero-stress SL relaxation leads to strain and stress decreases; pressure drops to minimum. This phase is short. It was also skipped in our model which jumps from Phase 3 to Phase 1. The computational models were used to assess the effect of patch stiffness and thickness with the ultimate goal of finding out optimal patch design and location for myocardium regeneration.
- Our 2G model actually contains two sub-models: one for diastole phase (Phase 1), one for systole phase (Phase 3). The 2G model has continuous volume change, but discontinuous stress, strain and pressure changes, due to omissions of isovolumic Phases. An iterative pre-shrink process was applied to the in vivo minimum volume ventricular geometry to obtain the two zero-load geometries so that when in vivo pressure (begin-filling and end-systole pressure conditions, respectively) was applied, the ventricle would regain its in vivo geometry. Shrinking is achieved by shrinking each slice (short-axis direction) and reducing the slice distances (long-axis direction) with circumferential and longitudinal shrinkage rates determined by our iterative procedure. Different shrinkage rates were used for LV inner and outer surfaces so that mass conservation law was enforced. To get the zero-load diastole geometry, we start with a 4% shrinkage, construct the model, and apply the minimum pressure to see if the pressurized LV volume matches the echo data. If not, we adjust the shrinkage, re-made the model, pressurize it and check again. The process is repeated until LV volume matches echo volume with error < 0.5%. For the zero-load systole geometry, assuming a 10-15% sarcomere shortening, we start with a 14% shrinkage. The same process was repeated until the pressurized LV volume under end-systole pressure matched the echo-measured end-systole volume data. The systole and diastole models are really two different models, with equal LV volumes linking them to form a cardiac cycle.

### **2.3 The one zero-load geometry (1G) models**

The 1G models were introduced in our previous paper [Fan, Yao, Yang, et al. (2015)]. The modeling details are the same as the 2G models except that it uses only one zero-load geometry. The model starts from BF with minimum volume and pressure, goes to end-filling with maximum LV volume corresponding to maximum pressure (this is its main difference from 2G model), then returns to end-ejection with minimum LV volume and minimum pressure. Its systole phase was just a reversal of its diastole phase. LV material properties were adjusted to simulate active contraction and relaxation and match - measured LV volumes. The end-diastole and end-systole pressure conditions were

incorrectly imposed. That is why we are introducing the new 2G models to improve over the 1G models.

#### **2.4 Two-layer anisotropic LV model construction with fiber orientations**

The governing equations for the LV model were:

$$\rho v_{i,tt} = \sigma_{ij,j}, \quad i,j=1,2,3; \text{ sum over } j, \quad (1)$$

$$\epsilon_{ij} = (v_{i,j} + v_{j,i} + v_{\alpha,i} v_{\alpha,j})/2, \quad i,j,\alpha=1,2,3, \quad (2)$$

where  $\sigma$  is the stress tensor,  $\epsilon$  is the strain tensor,  $\mathbf{v}$  is displacement, and  $\rho$  is material density. The normal stress was assumed to be zero on the outer (epicardial) LV surface and equal to the pressure conditions imposed on the inner (endocardial) LV surfaces.

The ventricle material/infarct tissue was assumed to be hyperelastic, anisotropic/isotropic, nearly-incompressible and homogeneous. The nonlinear Mooney-Rivlin model was used to describe the nonlinear anisotropic and isotropic material properties. The strain energy function for the isotropic modified Mooney-Rivlin model is given by [Tang, Yang, Geva, et al. (2010); Tang, Yang, Geva, et al. (2011)]:

$$W = c_1(I_1 - 3) + c_2(I_2 - 3) + D_1 [\exp(D_2(I_1 - 3)) - 1], \quad (3)$$

where  $I_1$  and  $I_2$  are the first and second strain invariants given by,

$$I_1 = \sum C_{ii}, \quad I_2 = \frac{1}{2} [I_1^2 - C_{ij}C_{ij}], \quad (4)$$

$C = [C_{ij}] = X^T X$  is the right Cauchy-Green deformation tensor,  $X = [X_{ij}] = [\partial x_i / \partial a_j]$ ,  $(x_i)$  is the current position,  $(a_i)$  is the original position,  $c_i$  and  $D_i$  are material parameters chosen to match experimental measurements [Tang, Yang, Geva, et al. (2011); Humphrey(2002); xel (2002)]. The strain energy function for the anisotropic modified Mooney-Rivlin model was obtained [Tang D, Yang C, Geva T, et al. (2010)]:

$$W = c_1(I_1 - 3) + c_2(I_2 - 3) + D_1 [\exp(D_2(I_1 - 3)) - 1] + K_1 / (2K_2) \exp[K_2(I_4 - 1)^2 - 1], \quad (5)$$

where  $I_4 = C_{ij} (\mathbf{n}_f)_i (\mathbf{n}_f)_j$ ,  $C_{ij}$  is the Cauchy-Green deformation tensor,  $\mathbf{n}_f$  is the fiber direction,  $K_1$  and  $K_2$  are material constants. With parameters properly chosen, it was shown that stress-strain curves derived from Eq. (5) agreed very well with the stress-strain curves from the anisotropic (transversely isotropic) strain-energy function with respect to the local fiber direction given in [McCulloch, Waldman, Rogers, et al. (1992)]:

$$W = \frac{C}{2} (e^Q - 1), \quad (6)$$

$$Q = b_1 E_{ff}^2 + b_2 (E_{cc}^2 + E_{rr}^2 + E_{cr}^2 + E_{rc}^2) + b_3 (E_{fc}^2 + E_{cf}^2 + E_{fr}^2 + E_{rf}^2), \quad (7)$$

where  $E_{ff}$  is fiber strain,  $E_{cc}$  is cross-fiber in-plane strain,  $E_{rr}$  is radial strain, and  $E_{cr}$ ,  $E_{fr}$  and  $E_{fc}$  are the shear components in their respective coordinate planes,  $C$ ,  $b_1$ ,  $b_2$ , and  $b_3$  are parameters to be chosen to fit experimental data. For simplicity,  $b_1$ ,  $b_2$ , and  $b_3$  in Eq. (7) were kept as constants,  $C$  in Eq. (6) were chosen to fit echo-measured LV volume data.

As patient-specific fiber orientation data was not available from these patients, we chose

to construct a two-layer LV model and set fiber orientation angles using fiber angles given in [Axel(2002)]. Fiber orientation angles were set at -60 degrees and 80 degrees for epicardium (outer layer) and endocardium (inner layer), respectively. Fiber orientation can be adjusted when patient-specific data becomes available [Tang, Yang, Geva, et al. (2008)].

### ***2.5 A geometry-fitting technique for mesh generation***

A geometry-fitting mesh generation technique developed in our previous studies was also used to generate mesh for our models [Tang, Yang, Geva, et al. (2010)]. Mesh analysis was performed by decreasing mesh size by 10% (in each dimension) until solution differences were less than 2%. The mesh was then chosen for our simulations.

### ***2.6 Solution methods and data collection for statistical analysis***

The anisotropic LV computational models were constructed for the two groups and the models were solved by ADINA (ADINA R&D, Watertown, MA, USA) using unstructured finite elements and the Newton-Raphson iteration method. Because stress and strain are tensors, for simplicity, maximum principal stress (Stress- $P_1$ ) and strain (Strain- $P_1$ ) were used for analysis and referred to as stress and strain in this paper. For each LV model (1G and 2G for each subject,  $n=15$ ), the equivalent Young's modulus (YM) values at begin-filling, end-diastole, begin-ejection, end-systole in the fiber direction were calculated from the Mooney-Rivlin models for comparisons. For each LV data set (11 slices. Slices are short-axis cross sections), we divided each slice into 4 quarters, each quarter with equal inner wall circumferential length. Ventricle wall thickness, circumferential curvature, longitudinal curvature and stress/strain were calculated at all nodal points (100 points/slice, 25 points/quarter). The "quarter" values of those parameters were obtained by taking averages of those quantities over the 25 points for each quarter and saved for comparative analysis. Statistical analysis was performed using MATLAB R2011b. We applied the Kolmogorov-Smirnov test to check the normality, the test showed non-normal distribution. The comparative analysis for our 1G model and 2G models were performed using non-parametric Mann-Whitney U test. Patient group comparisons were performed using the non-parametric Kruskal-Wallis test. A  $p$ -value $<0.05$  was considered statistically significant.

## **3 Results**

In the following, BF, ED, BE and ES were used for Begin-Filling, End-Diastole, Begin-Ejection and End-Systole, respectively. For 1G models, ED and BE are identical. Therefore, 1G ED and BE have the same volume, pressure, and stress/strain conditions. The same is true for ES and BF. In a cardiac cycle, ventricle ED and BE conditions are different. 2G models improved over 1G model by using different zero-load diastole and systole geometries and different pressure conditions at ED and BE so that ED and BE stress/strain results from 2G models were considerably different. The situation for BF and ES was similar. This explanation should be helpful in understanding the model differences and results presented below.

### 3.1 LV diastolic and systolic material properties from 2G models

Myocardium material stiffness changes in a cardiac cycle. Material parameter values from 2G models ( $n=15$ ) at BF, ED, BE and ES are given in Table 2. Figure 3 gives the stress-stretch curves for 2G model from one patient (P1) to illustrate the material differences from the diastole and systole. For diastole phase, BF mean YM value in the fiber direction ( $YM_f$ ) was 738% higher than its ED value (645.39 kPa vs. 76.97 kPa,  $p=3.38E-06$ ). For systole phase, ES  $YM_f$  was 903% higher than its BE value (1025.10 kPa vs. 102.11 kPa,  $p=6.10E-05$ ). Comparing systolic and diastolic material properties, ES  $YM_f$  was 59% higher than its BF value (1025.10 kPa vs. 645.39 kPa,  $p=0.0002$ ).

**Table 2:** Material parameters from the 2G models. BF: Begin-Filling; ED: End-Diastole. BE: Begin-Ejection; ES: End-Systole.

	C(kPa)	$YM_f$ (kPa)	$YM_c$ (kPa)	C(kPa)	$YM_f$ (kPa)	$YM_c$ (kPa)
	<b>2G-BF</b>			<b>2G-ED</b>		
P1	18.942	544.62	188.32	2.3813	68.467	23.675
P2	25.978	746.91	258.27	2.3452	67.429	23.316
P3	21.648	622.43	215.22	3.1390	90.252	31.208
P4	19.122	549.81	190.11	2.8503	81.953	28.338
P5	19.844	570.56	197.29	2.1648	62.243	21.522
P6	28.864	829.91	286.97	1.7860	51.350	17.756
P7	31.570	907.70	313.87	1.5695	45.126	15.604
P8	21.648	622.43	215.22	4.4198	127.08	43.942
P9	46.904	1348.6	466.32	1.2628	36.308	12.558
P10	17.138	492.75	170.39	3.0127	86.621	29.952
P11	20.746	596.49	206.27	3.3013	94.920	32.822
P12	11.437	328.85	113.71	2.8323	81.434	28.159
P13	13.350	383.83	132.72	3.6982	106.33	36.768
P14	14.071	404.58	139.90	2.9946	86.102	29.773
P15	25.436	731.35	252.89	2.3993	68.986	23.854
<b>Mean</b>	<b>22.447</b>	<b>645.39</b>	<b>223.16</b>	<b>2.6771</b>	<b>76.973</b>	<b>26.616</b>
	<b>2G-BE</b>			<b>2G-ES</b>		
P1	2.4895	71.579	24.751	31.029	892.14	308.49
P2	2.6519	76.247	26.365	38.425	1104.81	382.02
P3	3.4998	100.63	34.795	32.652	938.82	324.63
P4	3.7523	107.89	37.306	31.390	902.52	312.07
P5	2.3272	66.911	23.137	33.735	969.95	335.39
P6	2.0205	58.093	20.088	38.786	1115.2	385.61
P7	1.8040	51.869	17.935	45.100	1296.7	448.38
P8	6.4944	186.73	64.567	37.884	1089.2	376.64
P9	1.3710	39.420	13.631	52.316	1504.2	520.12

P10	3.3194	95.439	33.001	34.637	995.88	344.36
P11	4.0049	115.15	39.817	38.425	1104.8	382.02
P12	4.3476	125.00	43.224	27.240	783.22	270.82
P13	5.9532	171.17	59.187	28.684	824.71	285.17
P14	5.9352	170.65	59.007	29.315	842.87	291.45
P15	3.3013	94.920	32.822	35.178	1011.4	349.74
<b>Mean</b>	<b>3.5515</b>	<b>102.11</b>	<b>35.309</b>	<b>35.653</b>	<b>1025.1</b>	<b>354.46</b>

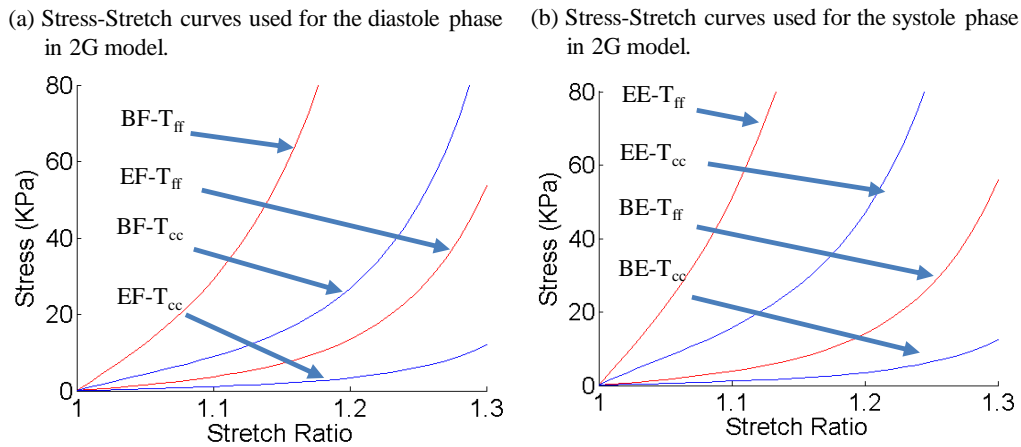


**Figure 3:** Material Stress-Stretch curves from 2G model of Patient 1. T<sub>ff</sub>: stress in fiber direction; T<sub>cc</sub>: stress in circumferential direction. BF: Begin-Filling; ED: End-Diastole. BE: Begin-Ejection; ES: End-Systole.

### 3.2 LV material properties from 1G models and comparison with 2G models

Our 1G model essentially treated the diastole and systole phases the same way, with material stiffness adjusted to match minimum and maximum LV volumes corresponding to minimum and maximum pressure conditions. Material parameter values from 1G model of 15 patients are given in Tables 3. Figure 4(a) gave Stress-Stretch Ratio plots from 1G model (Patient 1). Bar plots of mean  $YM_f$  values of the 15 patients from 1G and 2G models were given in Fig. 4 (b). Using the 1G model as the baseline values, BF  $YM_f$  from 2G models was 127% higher than that from the 1G model (645.39 kPa vs. 284.41 kPa,  $p=2.79E-05$ ). BE  $YM_f$  from 2G models was 34% lower than that from the 1G model (102.11 kPa vs. 154.81 kPa,  $p=0.020$ ). ES  $YM_f$  from 2G models was 260% higher than that from the 1G model (1025 kPa vs. 284.4 kPa,  $p=3.37E-06$ ). ED  $YM_f$  from 2G models was 37% lower than that from the 1G model (76.97 kPa vs. 154.81kPa,  $p=0.0007$ ). It should be noted that 1G model treated BF and ES as the same due to model simplifications. This indicated the material parameter properties from 2G models were stiffer than that from 1G model at BF and ES corresponding to minimum LV volume, and softer than that from 1G model at BE and ED corresponding to maximum LV volume.

**Table 3:** Material parameters from the 1G model. BF: Begin-Filling; BE: Begin-Ejection.

	C(kPa)	YM <sub>f</sub> (kPa)	YM <sub>c</sub> (kPa)	C(kPa)	YM <sub>f</sub> (kPa)	YM <sub>c</sub> (kPa)
	1G-BF			1G-BE		
P1	10.102	290.47	100.44	5.7367	164.94	57.034
P2	11.185	321.59	111.20	5.2857	151.98	52.551
P3	11.365	326.77	113.00	8.0278	230.82	79.812
P4	10.283	295.65	222.00	7.7211	102.23	76.763
P5	11.419	328.33	113.53	6.0073	172.72	59.725
P6	14.432	414.95	143.48	4.5100	129.67	44.838
P7	13.530	389.02	134.52	3.6621	105.29	36.409
P8	10.102	290.47	100.44	9.4710	272.31	94.161
P9	19.483	560.18	193.70	2.9586	85.065	29.414
P10	9.3808	269.72	93.264	7.3964	212.66	73.535
P11	6.9995	201.25	69.589	6.9634	200.21	69.230
P12	7.3603	211.62	73.176	6.9454	199.69	69.051
P13	2.9766	85.58	29.593	2.7060	77.803	26.903
P14	2.0385	58.61	20.267	1.8581	53.425	18.473
P15	7.7211	222.00	76.763	5.6826	163.39	56.496
<b>Mean</b>	<b>9.8919</b>	<b>284.41</b>	<b>106.33</b>	<b>5.6622</b>	<b>154.81</b>	<b>56.293</b>

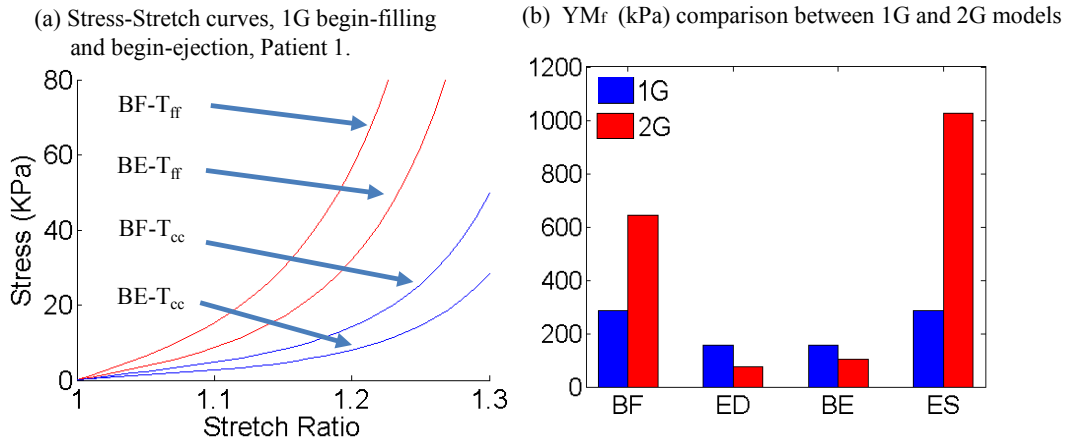


**Figure 4:** Material Stress-Stretch Ratio curves from 1G model (P1) and bar plots for 1G/2G comparisons. T<sub>ff</sub>: stress in fiber direction; T<sub>cc</sub>: stress in circumferential direction. BF: Begin-Filling; ED: End-Diastole; BE: Begin-Ejection; ESE: End-Systole.

### 3.3 LV diastolic and systolic stress/strain calculations from 2G models

Table 4 summarizes the mean stress/strain values of the 15 patients from 2G models. It should be noted that 2G models provide end-systole and end-diastole stress conditions which were not available from 1G models. The LV had the same volume at ED and BE,

but BE stress average value was 514% higher than its ED value (299.69 kPa vs. 48.81 kPa,  $p=3.39E-06$ ), BE strain average value was 31.5% higher than its ED value (0.9417 vs. 0.7162,  $p=0.004$ ). Similarly, the LV had their minimum volumes at both ES and BF, ES stress average value was 562% higher than its BF value (19.74 kPa vs. 2.98 kPa,  $p=6.22E-05$ ). ES strain average value was 264% higher than its BF value (0.1985 vs. 0.0546,  $p=3.42E-06$ ). We are able to get those values because we used different zero-load geometries for diastole and systole phases, respectively.

**Table 4:** Average stress results from 2G models. BF: Begin-Filling; BE: Begin-Ejection; ED: End-Diastole; ES: End-Systole.

Patient	Stress (kPa)				Strain			
	2G-BF	2G-ED	2G-BE	2G-ES	2G-BF	2G-ED	2G-BE	2G-ES
P1	1.9345	47.986	311.31	15.429	0.0508	0.7820	1.0297	0.2120
P2	2.6241	58.033	372.43	17.785	0.0502	0.7972	1.0360	0.2021
P3	2.0071	37.989	265.97	15.331	0.0497	0.7437	1.0135	0.2172
P4	1.8084	30.841	255.31	14.907	0.0496	0.7150	0.9860	0.2145
P5	2.3700	62.283	401.50	16.690	0.0613	0.8437	1.0948	0.2185
P6	2.0724	64.571	353.67	13.015	0.0393	0.9049	1.1325	0.1700
P7	1.7388	74.045	363.51	12.619	0.0291	0.9102	1.1110	0.1403
P8	2.8673	41.191	261.85	18.875	0.0615	0.6632	0.8768	0.2042
P9	2.6838	105.48	495.94	15.139	0.0289	0.9904	1.2036	0.1403
P10	2.5062	57.221	370.09	19.644	0.0684	0.7598	1.0053	0.2227
P11	6.0850	38.362	260.44	36.875	0.0565	0.4988	0.7060	0.1962
P12	2.8688	29.262	198.11	19.765	0.0914	0.6297	0.8362	0.2358
P13	4.4181	24.594	176.21	26.681	0.0787	0.4886	0.6947	0.2240
P14	5.4052	26.284	169.66	30.958	0.0634	0.4052	0.5695	0.1924
P15	3.3359	34.033	239.36	22.434	0.0401	0.6112	0.8299	0.1866
<b>Mean</b>	<b>2.9817</b>	<b>48.812</b>	<b>299.69</b>	<b>19.743</b>	<b>0.0546</b>	<b>0.7162</b>	<b>0.9417</b>	<b>0.1985</b>

### 3.4 LV stress/strain calculations from 1G models and comparison with 2G models

Table 5 summarizes the average stress/strain values of the 15 patients from 1G model. Figure 4 shows the stress/strain plots from 1G and 2G models at BE using the patient given by Fig. 1 as an example. Bar plots of mean stress/strain values of the 15 patients from 1G and 2G models were in Fig. 4 (c) and (f) showing clear comparisons. BE mean stress value from the 2G models was 22% higher than that from the 1G model (299.69 kPa vs. 246.26 kPa,  $p=0.004$ ), while ED mean stress value from the 2G models was 80% lower than that from the 1G model (48.8 kPa vs. 246.26 kPa,  $p=6.22E-06$ ). BE mean strain value from the 2G models was 10% higher than that from the 1G model (0.9417 vs. 0.8547,  $p=0.007$ ), while ED mean strain value from the 2G models was 16.2% lower than that from the 1G model (0.7162 vs. 0.8547,  $p=0.02$ ). BF stress and strain values from 1G and 2G models were much lower than those at BE and relative percentage differences may not be as important.

**Table 5:** Average strain results from 1G model. BF: Begin-Filling; BE: Begin-Ejection

Patient	Stress (kPa)		Strain	
	1G-BF	1G-BE	1G-BF	1G-BE
P1	2.3290	224.68	0.1121	0.8845
P2	2.8488	293.62	0.1228	0.9206
P3	2.3849	185.83	0.1103	0.8492
P4	2.4531	186.16	0.1215	0.8438
P5	2.5214	290.74	0.1110	0.9293
P6	2.2008	277.08	0.0826	0.9910
P7	1.8442	292.55	0.0716	0.9935
P8	3.4650	221.26	0.1514	0.8061
P9	2.7979	408.15	0.0726	1.0780
P10	2.6982	276.19	0.1292	0.8654
P11	7.1837	209.58	0.1630	0.6312
P12	3.8025	157.38	0.1767	0.7521
P13	6.3681	235.75	0.3279	0.8229
P14	8.3351	240.00	0.3223	0.7070
P15	3.8301	194.98	0.1336	0.7459
<b>Mean</b>	<b>3.6708</b>	<b>246.26</b>	<b>0.1472</b>	<b>0.8547</b>

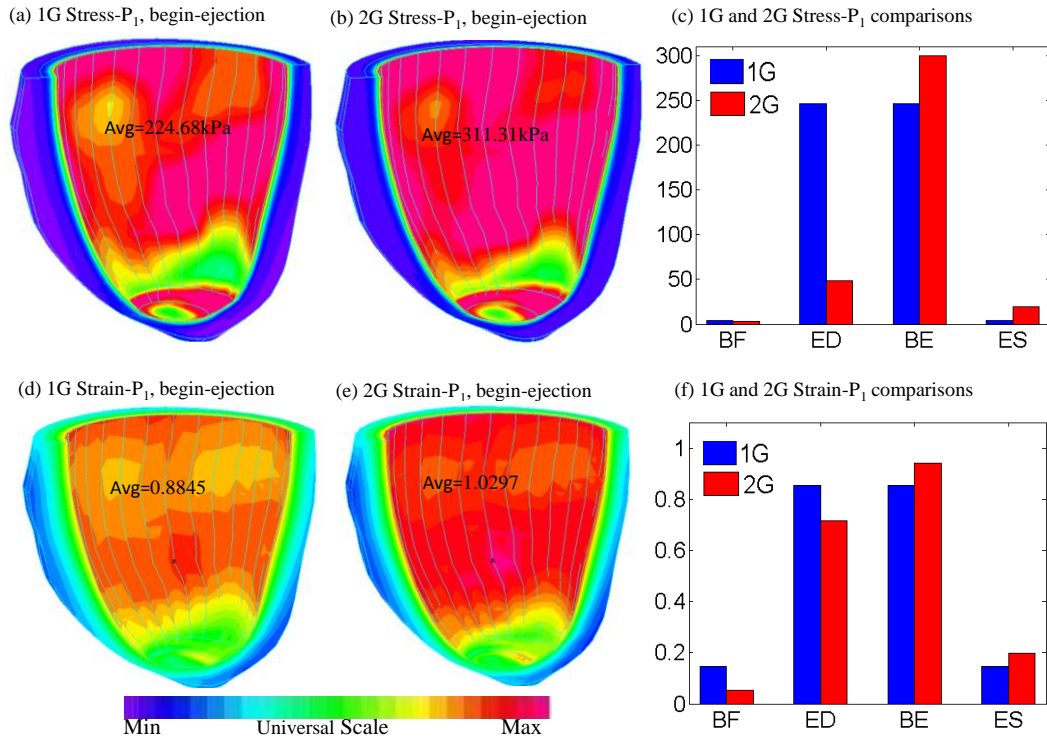


**Figure 5:** Stress and strain plots from the 2G and 1G models showing large differences.

### 3.5 Group comparison using 2G models

Table 6 summarizes the comparison of LV WT, C-curvature, L-curvature, and stress/strain values between the two groups (IG and NIG) at BF, ED, BE, and ES using 2G model results. Figure 5 give the bar plots for the five parameters and  $YM_f$ . It shows that stress, strain and L-curvature had most noticeable differences between the two groups; C-curvature also had clear differences, while  $YM_f$  needed closer check. At BE, using NIG (healthy controls) values as the base, LV stress and strain from IG were 39.5% and 30.5% lower than that from NIG, respectively. It is more worth noting that LV stress and strain variation from BE to ES from IG were 55% (181.5 kPa vs. 329.3 kPa) and 30.5% (0.52 vs. 0.86) lower than that from NIG. At ED, LV stress and strain from IG were 47.3% and 34.6% lower than that from IG (30.5 kPa vs. 58.0 kPa; 0.53 vs. 0.81). LV stress and strain variation from BF to ED from IG were 53% (26.1 kPa vs. 55.74 kPa) and 29.5% (0.46 vs. 0.76) lower than that from NIG. L-curvature from IG were 68%, 75%, 81% and 71% higher than that from NIG at BF, ED, BE and ES, respectively. C-curvature from IG were 27.3%, 17.2%, 18.6% and 28.7% lower than that from NIG at BF, ED, BE and ES. For material properties,  $YM_f$  variation from IG during BE and ES was 22% lower than that from NIG (778 kPa vs. 995.5 kPa).  $YM_f$  variation from IG during BF and ED was 38.5% lower than that from NIG (401 kPa vs. 652 kPa). Reduction of  $YM_f$  variation is the reflection of loss of contractility.

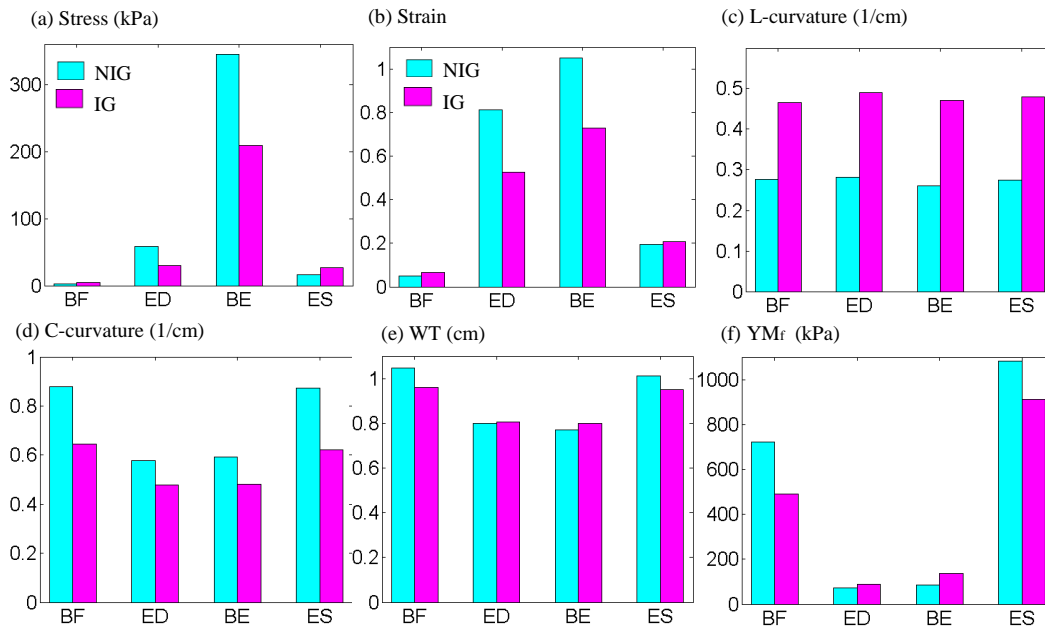


**Figure 6.** Bar plots for Material parameters ( $YM_f$ ), LV wall thickness (WT), circumferential curvature, longitudinal curvature and stress/strain values between Non-Infarct Group and Infarcted Group. NIG: Non-Infarct Group (light blue); IG: Infarcted Group (purple).

**Table 6:** Comparison of LV Material parameters (YM<sub>f</sub>), wall thickness, circumferential and longitudinal curvature and stress/strain between Non-Infarct Group (NIG) and Infarcted Group (IG) at begin-filling, end-diastole, begin-ejection, and end-systole.

	Begin-Filling				End-Diastole			
	IG	NIG	%	P-value	IG	NIG	%	P-value
YM <sub>f</sub> (kPa)	489 ±169	723.6 ±257	67.6	0.0706	87.6 ±14.1	71.7 ±26.3	122	0.1645
WT (cm)	0.96 ±0.18	1.05 ±0.23	91.4	0.0178	0.81 ±0.16	0.80 ±0.19	101	0.7309
C-cur (1/cm)	0.64 ±0.37	0.88 ±0.40	72.7	3.40E-08	0.48 ±0.28	0.58 ±0.30	82.8	0.0006
L-cur (1/cm)	0.47 ±0.27	0.28 ±0.22	168	4.76E-06	0.49 ±0.35	0.28 ±0.18	175	1.32E-05
Stress (kPa)	4.42 ±2.05	2.26 ±0.52	196	1.68E-16	30.5 ±8.16	58.0 ±23.9	52.6	8.16E-17
Strain	0.07 ±0.03	0.05 ±0.02	140	8.55E-05	0.53 ±0.18	0.81 ±0.15	65.4	1.12E-16
	Begin-Ejection				End-Systole			
	IG	NIG	%	P-value	IG	NIG	%	P-value
YM <sub>f</sub> (kPa)	135.4 ±34.2	85.5 ±41.8	158	0.0400	913.4 ±138	1081 ±193	84.5	0.1032
WT (cm)	0.80 ±0.16	0.77 ±0.19	104	0.5838	0.95 ±0.17	1.01 ±0.21	94.1	0.0652
C-cur (1/cm)	0.48 ±0.30	0.59 ±0.31	81.4	8.19E-05	0.62 ±0.38	0.87 ±0.42	71.3	1.26E-08
L-cur (1/cm)	0.47 ±0.34	0.26 ±0.17	181	3.42E-06	0.48 ±0.29	0.28 ±0.20	171	1.70E-06
Stress (kPa)	208.8 ±60.0	345.2 ±96.0	60.5	3.67E-16	27.3 ±8.96	15.9 ±3.51	172	1.05E-18
Strain	0.73 ±0.21	1.05 ±0.16	69.5	1.16E-16	0.21 ±0.07	0.19 ±0.05	111	0.1782

## **4 Discussion**

### ***4.1 Significance of the new 2G models***

Correct stress/strain calculation is of fundamental importance for many cardiovascular research where mechanical forces play a role. Ventricle remodeling, disease development, tissue regeneration, patient recovery after surgery and many other cell activities are closely associated with ventricle mechanical conditions. The 2G modeling approach is setting up the right stage for diastole and systole stress/strain calculations using proper zero-load geometries. 1G model do not use different reference geometries for systole and diastole phases, therefore have difficulties in giving right strain calculations. It should be noted that direct measurements of stress, strain, and zero-load sarcomere length are either extremely difficult or even impossible. Even by using tagging, the strain determined uses in vivo references and could not account for zero-stress SL changes. Actual ventricle contraction and relaxation are very complex. Our model is only a first-order approximation, an improvement over the 1G model. Lack of in vivo data and model construction cost are also considerations. Data from the literature or from ex vivo experiments have to be used to complete the computational models. We are in need of patient-specific data such as fiber orientation, sarcomere length contraction rate, regional material properties, etc.

### ***4.2 Comparison of our new models with existing models in the literature***

Stress/strain calculation requires correct reference geometry. Without correct reference geometry, stress/strain cannot even start. However, during cardiac active contraction and relaxation, ventricle reference geometry keeps changing due to sarcomere contraction. That is why we introduced our 2G model approach, which is an attempt to treat ventricle diastole and systole phases separately with different zero-load geometries. Most current ventricle models (including our own models referred to 1G models) use one reference geometry. Stress/strain calculations from those 1G models will contain errors associated with the incorrect reference geometries and possibly other wrong model assumptions (such as improper pressure conditions).

### ***4.3 Clinical implications***

Section 3.5 compared stress/strain conditions and YM values between the Infarct Group (IG) and Non-Infarct Group (NIG).LV stress and strain variation from BE to ES from IG were 55% and 30.5% lower than that from NIG.  $YM_f$  variation from IG during BF and ED was 38.5% lower than that from NIG. These results gave us some hope that stress/strain conditions and material parameter values from our models could be used to identify patients who had infarct (possibly unnoticed by patients themselves). More studies are needed to confirm our findings.

### ***4.4 Model limitations***

Model limitations include the following: a) ventricle valve mechanics was not included. Valve mechanics plays an important role. However, including it will require considerable more data and modeling effort; b) fluid-structure interaction was not included; c) local ventricle deformation imaging data (by particle tracking) was not included; such data will

be very useful for determining tissue material properties and infarct area; d) active contraction and expansion were modeled by our two-phase model with material stiffening and softening without adjusting zero-stress ventricle geometries.

**Acknowledgment:** This research was supported in part by National Heart, Lung and Blood Institute grants R01 HL089269, National Sciences Foundation of China grants 11672001 and 81571691. LonglingFan's research is supported in part by the Fundamental Research Funds for the Central Universities (KYLX15\_0110) and the Scientific Research Foundation of Graduate School of Southeast University (YBJJ1617).

## References

- Ambrosi, D.; Pezzuto, S.** (2012): Active Strain in Mechanobiology: Constitutive Issues. *J. Elast*, vol.107, pp.199–212.
- Axel L.** (2002): Biomechanical dynamics of the heart with MRI. *Annu. Rev. Biomed. Eng*, vol.4, pp.321-347.
- Costa, K. D.; Takayama, Y.; McCulloch, A. D.; Covell, J.W.** (1999): Laminar Fiber Architecture and Three-Dimensional Systolic Mechanics in Canine Ventricular Myocardium. *Am. J. Physiol*, vol.276, pp.H595-607.
- Fan, L. L.; Yao, J.; Yang, C.; Tang, D.; Xu, D.** (2015): Infarcted Left Ventricles Have Stiffer Material Properties and Lower Stiffness Variation: 3D Echo-Based Modeling to Quantify In Vivo Ventricle Material Properties. *J. Biomech. Eng*, vol.137, no.8, pp.081005.
- Fomovsky, G. M.; Macadangdang, J. R.; Ailawadi, G.; Holmes, J. W.** (2011): Model-based design of mechanical therapies for myocardial infarction. *J. Cardiovasc Transl Res*, vol.4, no.1, pp.82-91.
- Guccione, J. M.; McCulloch, A. D.** (1993a): Mechanics of active contraction in cardiac muscle: Part I—Constitutive relations for fiber stress that describe deactivation. *J. Biomech. Eng*, vol.115, no.1, pp.72–81.
- Guccione, J. M.; Waldman, L. K.; McCulloch, A. D.** (1993b): Mechanics of active contraction in cardiac muscle: Part II—Cylindrical models of the systolic left ventricle. *J. Biomech. Eng*, vol.115, no.1, pp.82–90.
- Holmes, J. W.; Costa, K. D.** (2006): Imaging cardiac mechanics: what information do we need to extract from cardiac images? *Conf Proc IEEE Eng Med Biol, Soc.* vol.1, pp.1545-1547.
- Humphrey, J. D.; Strumpf, R. K.; Yin, F. C.** (1999): Biaxial mechanical behavior of excised ventricular epicardium. *Am. J. Physiol*, vol.259, pp. H101-108.
- Humphrey, J. D.** (2002): *Cardiovascular Solid Mechanics: Cells, Tissues, and Organs*. Springer-Verlag, New York.
- Hunter, P. J.; Pullan, A. J.; Smaill, B. H.** (2003): Modeling total heart function. *Annu Rev Biomed Eng*, vol.5, pp.147-77.
- Kerckhoffs, R. C. P.; Healy, S. N.; Usyk, T. P.; McCulloch, A. D.** (2006): Computational methods for modeling cardiac electromechanics. *Proc IEEE*, vol. 94, pp.769-783.

- Liu, Y.; Wang, G.; Sun, L. Z.** (2006): Anisotropic elastography for local passive properties and active contractility of myocardium from dynamic heart imaging sequence. *Int J Biomed Imaging*, vol. 2006, pp.459-57.
- McCulloch, A. D.; Waldman, L.; Rogers, J.; Guccione, J. M.** (1992): Large-scale finite element analysis of the beating heart. *Critical Rev. in Biomed. Eng*, vol.20, no.(5, 6), pp. 427-449.
- McCulloch, A. D.** (2007): Continuity 6 (a package distributed free by the National Biomedical Computation Resource), [www.continuity.ucsd.edu](http://www.continuity.ucsd.edu).
- Moulton, M. J.; Secomb, T. W.** (2013): A low-order model for left ventricle dynamics throughout the cardiac cycle. *Math Med Biol*, vol.30, no.1, pp.45-63.
- Nash, M. P.; Hunter, P. J.** (2000): Computational Mechanics of the Heart, From Tissue Structure to Ventricular Function. *Journal of Elasticity*, vol. 61, pp.113-41.
- Peskin, C. S.** (1997): Numerical analysis of blood flow in the heart. *J Com Phys*, vol. 25, pp.220-252.
- Pezzuto, S.; Ambrosi, D.**(2014): Active contraction of the cardiac ventricle and distortion of the microstructural architecture. *Int J.Numer Method Biomed Eng*, vol.30, no.12, pp.1578-1596.
- Pfeiffer, E.; Tangney, J. R.; Omens, J. H.; McCulloch, A. D.** (2014): Biomechanics of cardiac electromechanical coupling and mechanoelectric feedback. *J. Biomech. Eng*, vol. 6, no.2, pp.021007.
- Rogers, J. M.; McCulloch, A. D.**(1994): Nonuniform Muscle Fiber Orientation Causes Spiral Wave Drift in a Finite Element Model of Cardiac Action Potential Propagation. *J. Cardiovasc. Electrophysiol*, vol. 5, no.6, pp.496-509.
- Rossi, S.; Ruiz-Baier, R.; Pavarino, L. F.; Quarteroni, A.** (2012): Orthotropic active strain models for the numerical simulation of cardiac biomechanics. *Int J.Numer Method Biomed Eng*, vol. 28, no. 6-7, pp.761-88.
- Sacks, M. S.; Chuong, C.**(1993): Biaxial Mechanical Properties of Passive Right Ventricular Free Wall Myocardium. *J. Biomech. Eng*, vol.115, pp.202-205.
- Takayama, Y.; Costa, K. D.; Covell, J. W.** (2002): Contribution of Laminar Myofiber Architecture to Load-Dependent Changes in Mechanics of LVMyocardium. *Am J Physiol Heart CircPhysiol*, vol.282, no.4, pp. H1510-1520.
- Tang, D.; Yang, C.; Geva, T.; del Nido, P. J.** (2008): Patient-specific MRI-based 3D FSI RV/LV/Patch models for pulmonary valve replacement surgery and patch optimization. *J. of Biomech. Engineering*, vol.130, no.4, pp. 041010.
- Tang, D.; Yang, C.; Geva, T.; del Nido, P. J.** (2010): Image-Based Patient-Specific Ventricle Models with Fluid-Structure Interaction for Cardiac Function Assessment and Surgical Design Optimization. *Progress in Pediatric Cardiology*, vol. 30, pp.51-62.
- Tang, D.; Yang, C.; Geva, T.; Gaudette, G.; del Nido, P. J.** (2011): Multi-physics MRI-based two-layer fluid-structure interaction anisotropic models of human right and left ventricles with different patch materials: cardiac function assessment and mechanical stress analysis. *Computers & Structures*, vol. 89, pp.1059-1068.

**Tang, D.; del Nido, P. J.; Yang, C.; Zuo, H.; Huang, X. Y.; Rathod, R. H.; Tang, A.; Wu, Z. Y.; Billiar, K. L.; Geva, T.** (2016): Patient-Specific MRI-Based Right Ventricle Models Using Different Zero-Load Diastole and Systole Geometries for Better Cardiac Stress and Strain Calculations and Pulmonary Valve Replacement Surgical Outcome Predictions. *PLOS One*, vol.11, no.9, pp.e0162986.

**Wang, V. Y.; Lam, H. I.; Ennis, D. B.; Cowan, B. R.; Young, A. A.; Nash, M. P.** (2010): Cardiac Active Contraction Parameters Estimated from Magnetic Resonance Imaging. *STACOM-CESC*, vol.6364, pp.194–203.